102567
#1

Variable-Fidelity Hypersonic Aeroelastic Analysis of Thin-Film Ballutes

Reuben R. Rohrschneider and Robert D. Braun
Guggenheim School of Aerospace Engineering
Georgia Institute of Technology
270 Ferst Dr., Atlanta, GA 30332-0150

ABSTRACT

Many authors have shown the potential mass savings that a ballute can offer for both aerocapture and entry. This mass savings could enhance or even enable many scientific and human exploration missions. Prior to flight of a ballute several technical issues need to be addressed, including aeroelastic behavior. This paper begins to address the issue of aeroelastic behavior by developing and validating the Ballute Aeroelastic Analysis Tool (BAAT). The validation effort uses wind tunnel tests of clamped ballute models constructed of Kapton supported by a rigid nose and floating aft ring. Good correlation is obtained using modified Newtonian aerodynamics and non-linear structural analysis with temperature dependent material properties and thermal expansion. BAAT is then used to compute the deformed shape of a clamped ballute for Titan aerocapture in both the continuum and transitional regimes using impact method aerodynamics and direct simulation Monte Carlo.

NOMENCLATURE

C_p	- Pressure coefficient
Kn	- Knudsen number
nbmin	- Minimum number of flow cells on the body
q	- Dynamic pressure (Pa)
γ	- Ratio of specific heats

INTRODUCTION

The concept of the ballute has been around since the early 1960's and was first proposed for aerocapture in 1981 [1,2]. These initial ballutes were constructed of coated fabrics and often required flexible thermal protection. A significant break-through was made by McRonald when he discovered that increasing the ballute size to obtain a ballistic coefficient of 1 kg/m^2 or less would decrease the heat rate to order 1 W/cm^2, at which point polymer materials could be used to construct the ballute [3]. This advance was made possible by materials developed in the 1980's and led to a resurgence of interest in ballutes. In Rohrschneider and Braun [4] the current state-of-the-art is explored and technology gaps are identified in the areas of radiative heating and aeroelastic analysis. Hall [5] also concludes that coupled analysis is necessary when analyzing ballutes.

This paper begins to address the requirement for coupled analysis of ballutes and fully automates the coupling of non-linear structural analysis and hypersonic aerodynamics in the

continuum, rarefied, and transitional regimes. The coupled code is validated using wind tunnel tests performed by the In-Space Propulsion group at NASA Marshall, and shows good agreement when temperature dependent material properties and thermal expansion effects are included. Finally, a ballute for Titan aerocapture is analyzed in the continuum regime at the peak dynamic pressure point on the trajectory and in the transitional regime.

THE BALLUTE AEROELASTIC ANALYSIS TOOL

Coupling of aeroelastic problems can be divided into loosely coupled methods [6] which allow use of existing codes with little or no modification, and monolithic or fully integrated methods [7] which require a complete code rewrite.

Loosely coupled methods typically use existing analysis codes, rely on input and output files for data transfer, and don't necessarily exchange data at the end of each aerodynamic or structural dynamic analysis time step [8]. This allows for use of validated codes, substitution of other analysis codes, and simple coupling through the use of boundary conditions. Monolithic methods start with the governing equations of the problem and solve them simultaneously using a custom built solution algorithm. This requires a reformulation of the governing equations for compatibility [9], and since the source code is typically written in-house, tweaking is possible but validation is much more difficult.

The loose coupling method has been chosen for this application due in part to time constraints, lower complexity, and the desire to use validated codes. The method is also more modular and can be adapted more easily for variations on the problem and advances made in each discipline's analysis.

The analysis of thin-film ballutes requires structural dynamics and aerothermodynamics in the rarefied, transitional and continuum regime. Existing tools were chosen where available to eliminate the need to fully validate each individual analysis code. For all analyses a text file interface and command line execution are required for ease of integration into the interface code. Alternatively, analyses developed for this project can be run as sub-functions to the interface code, allowing data passing through memory.

Structural Analysis

The structural dynamics analysis needs to analyze geometrically non-linear deformation of thin polymer films with temperature dependent material properties. Several commercial codes were evaluated. LS-DYNA [10] performed the best and produced consistent answers where other codes encountered numerical stability problems. Solutions to thin-film problems in LS-DYNA are straightforward, requiring few additional inputs to achieve stability. The resulting displacement, velocity, and acceleration are produced at the nodes and temperatures and shear forces are input at nodes, while pressures are input at element face centers.

To ensure that the proper parameters are used in LS-DYNA for the coupled problem an inflated column buckling problem was computed and compared to experimental results published by Topping [11]. The experiment that most closely represents a thin-film ballute construction is a 0.0005 inch thick Mylar column inflated to 4.89 psi. Several element formulations and material models were used in LS-DYNA in an attempt to find the best modeling parameters for thin inflated membrane structures.

The buckling load from experiment was found to be 5.45 lb. by Topping and most of the element and material model combinations produced buckling loads between 5.28 and 5.37 lb. The

notable exception is the membrane model which produces buckling loads of 8.76 lb, much higher than the experimentally observed value. This is likely due to the inability of the membrane model to produce a moment which initiates buckling in the numerical model. Due to the fast run time, the fabric model with 10% liner thickness is used when thermal effects are not being considered and the elastic thermal model with a Belytschko-Tsay shell is used when thermal effects are included.

Aerodynamic Analysis

Continuum aerodynamics will be calculated by NASCART-GT [12,13] which is capable of handling moving boundary conditions and flow chemistry in the hypersonic flight regime. Various equation sets are available including Navier Stokes, Euler, or modified Newtonian. The analysis can run on multiple processors for static grid cases, but only a single processor when grid motion is involved. NASCART-GT uses a Cartesian grid and the only required geometric input is a triangulated surface. Currently, all data is output at the nodes and pressures are interpolated to obtain cell-centered values for input to LS-DYNA.

DAC [14] will be used for the rarefied and transitional aerodynamics, and was obtained from the Technology Transfer & Commercialization Office at NASA Johnson Space Center. The analysis is based on the Direct Simulation Monte Carlo method of Bird [15]. Flow chemistry is available if reaction equations are provided. Furthermore this method produces good solutions for any flow speed with high Knudsen number. DAC uses a Cartesian grid method with manually driven grid refinement based on the cell size to mean free path ratio. Results are produced at the surface nodes and pressures are interpolated to the face centers.

Due to the long computation time required by both NASCART-GT and DAC, a simplified set of aerodynamic tools is also being used. In the continuum regime, the modified Newtonian method [16] has been implemented, and in the rarefied regime the collisionless DSMC [15] method is used. The transitional regime is covered by use of a bridging function [17] of the form:

$$C_{p,bridge} = C_{p,cont} + \left(C_{p,fm} - C_{p,cont}\right)\sin^2\left\{\pi\left[A + \left(\tfrac{1}{2} - A\right)\log_n\left(Kn\right)\right]\right\}$$

Here A and n are found by fitting the CFD and DSMC results calculated by Peter Gnoffo and Richard Wilmoth of NASA Langley Research Center for the toroidal trailing ballute at Titan [18]. Coefficients were found that minimized the square of the difference between the bridging function and the actual results. The continuum and rarefied limits were also allowed to vary. The resulting values for A, n, and the bounds are presented in Table 1. Of note is the low value of the continuum limiting Knudsen number which is 0.00049, lower than the typical limit of 0.001 [19].

Table 1: Optimized bridging function parameters.

Parameter	Optimized Value
A	0.436
n	3.044
Kn_{upper}	3.044
Kn_{lower}	0.00049

Coupling Method

Coupling the analysis codes requires a scheme for transferring boundary condition data between the disparate analyses with as little interpolation error as possible. The most direct approach will be used here: direct node matching.

LS-DYNA uses primarily four-node shell elements while DAC and NASCART-GT require a pure three-node shell element input. Since both DAC and NASCART-GT only require surface resolution from the input grid, this can be satisfied by simply splitting the four-node elements from the LS-DYNA input. This allows simple data transfer since all analysis codes utilize the same node set. Interpolation over a single element is needed only for pressure data between DAC, NASCART-GT, and LS-DYNA where shell centered data is required. Interpolation from the aerodynamic grid to the structural dynamic grid requires area weighted averaging from two three-node elements to a single four-node element. Interpolation from nodal data to element centered data is done by averaging the surrounding nodal data which assumes the elements have nearly equal length edges.

BAAT VALIDATION STUDY

Validation of thin-film structures in a hypersonic flight condition is difficult due to the small amount of available data. To date, only two relevant tests have been performed, and only one provided deformation profiles. The first test aimed to demonstrate that a thin-film polymer could survive hypersonic flight conditions and to measure deflections of the membrane under load. The second test acquired qualitative temperature data on the membrane surface and would have provided quantitative temperatures and deformation profiles, but testing was cut short due to funding issues.

Geometry and Flight Conditions

Both tests were performed at the NASA Langley Research Center under contract from the In-Space Propulsion group at NASA Marshall Spaceflight Center [20]. The first tests used both the hypersonic CF_4 tunnel and the 31 inch Mach 10 Air tunnel, and the second test only used the Mach 10 Air tunnel. This validation study selected run 15 (6 inch diameter model, 1 mil Kapton membrane, CF_4 tunnel) from the first set of tests because it is a 6 inch model, the shock structure is visible in the available photograph, and the dynamic pressure and heat rate are lower. The lower dynamic pressure should minimize thermal effects in the results, leading to a better chance of predicting the deformed shape.

The geometry for the wind tunnel test is based on the clamped ballute configuration and has a rigid nose and rigid outer support with a membrane stretched between. The outer support is allowed to float axially to allow for axial deformation that is expected in flight. The outer diameter of the model is 15.24 cm and the rigid nose diameter is 1.3 cm. Figure 1 shows the test model prior to testing. The membrane is constructed of 0.254 mm (0.001 in.) thick Kapton and forms a 60 deg. half angle cone with one seam. During testing the seam was placed on the opposite side of the model from the camera so as to have the smallest affect on the results possible. Deformation data is from photographs of the model during testing. No dynamic data is available. Figure 2 shows an example photograph of the deformed profile during testing and the wrinkle pattern observed after testing. Because some of the membrane deformation remains after the loading is removed one or more of creep, plasticity, or thermal setting phenomenon take place in the test model. None of these effects are captured in the computational models and so exact deformations will not be reproduced, but qualitatively the deformed shape should be similar.

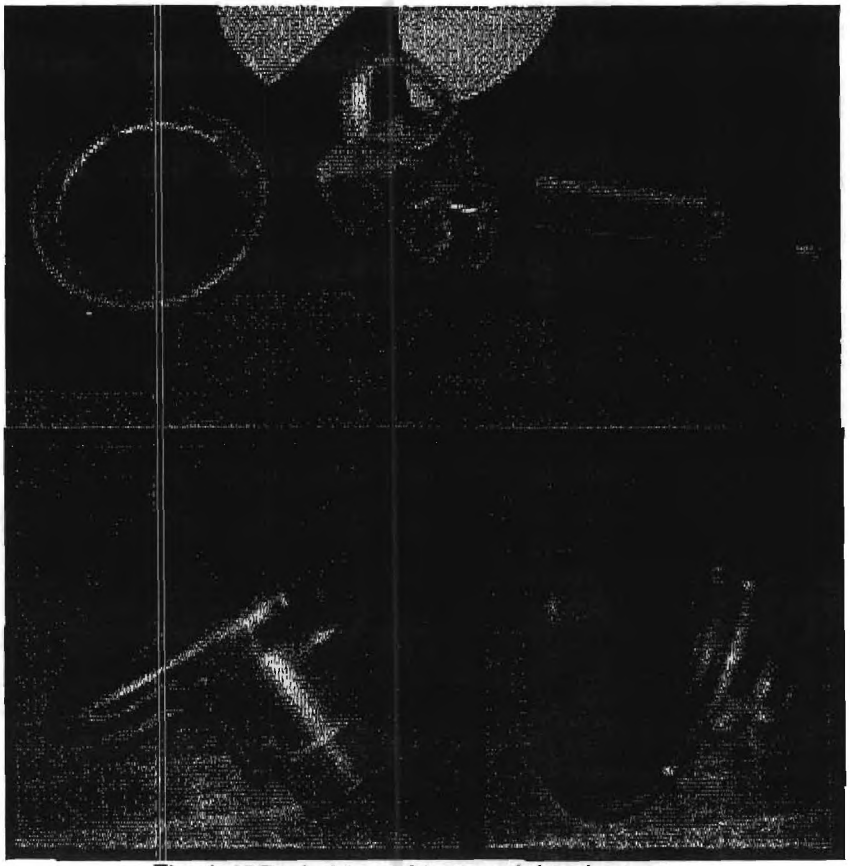

Fig. 1: ISP wind tunnel test models prior to use.

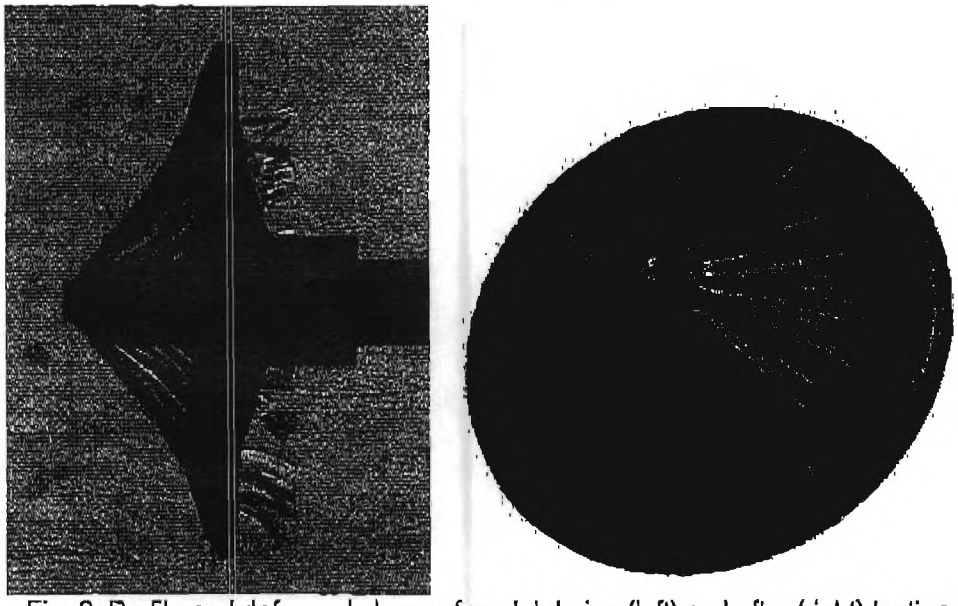

Fig. 2: Profile and deformed shape of model during (left) and after (right) testing.

The flight conditions are representative of hypersonic flight on Titan, but do not match any specific point on a calculated ballute trajectory. Table 2 shows the test conditions and the flight conditions of a clamped ballute at peak dynamic pressure. The test conditions have a higher

dynamic pressure than the calculated ballute trajectory leading to larger forces on the test model. The resulting Knudsen number is 0.00046, which is within the continuum regime, making this a useful validation case for the modified Newtonian method and NASCART-GT.

Table 2: CF_4 tunnel test conditions and Titan aerocapture flight conditions.

	CF_4 Test	Clamped Ballute @ Peak q
Dynamic Pressure (Pa)	654.0	51.5
Density (kg/m^3)	1.46×10^{-3}	5.66×10^{-6}
Temperature (K)	254.0	166.4
Velocity (m/s)	945.0	4226.4
Sonic Speed (m/s)	168.0	259.9

Structural Model & Grid Convergence Study

A finite element model was created of the wind tunnel test article using quadrilateral elements. Only one quarter of the model was used for computation due to the global symmetry of deformation and the local wrinkling of the surface. The membrane is modeled using the fabric material model with a 10% liner and the nose and aft support ring are assumed to be rigid. The model is fully constrained from the nose and the aft ring is constrained radially. The membrane is constructed of Kapton and was estimated to be at 260°C by the test engineer (Greg Buck of NASA Langley). Experimental data for the modulus of elasticity is available at 23°C, 200°C and 500°C and was linearly interpolated to obtain the value at 260°C. At the estimated temperature the modulus is 1.479 GPa and the poisson's ratio is 0.34 [21]. Due to the lack of temperature data from the test, the surface temperature is assumed to be uniform over the membrane.

The base model has 12 circumferential and 10 radial elements to simulate one quarter of the membrane, producing a fairly coarse model. Four different refinement levels were made that increase the number of elements used to simulate the membrane from 120 up to 4,992. Several solution metrics were tracked, including the number of surface wrinkles formed, the maximum principle stress, and the maximum axial deflection. Figure 3 shows the deformed grid on the "Fine" model which uses 1,920 elements to model the membrane. For the finest grid the number of circumferential elements is doubled as you move from the center outward. This was done to keep the minimum edge length a reasonable size since smaller edges produce smaller timesteps and longer run times. The models were run until a steady state was reached with a uniform pressure applied to the membrane (not coupled to aerodynamic analysis). Figure 4 shows that the "Fine" and "XFine" models have converged for both axial deflection and principle stress, but the number of wrinkles continues to bounce between 3 and 4. The variation in number of wrinkles between 3 and 4 does not appear to impact the displacement or stress significantly, and so is considered converged. Further computations will use the fine model with 1,920 elements.

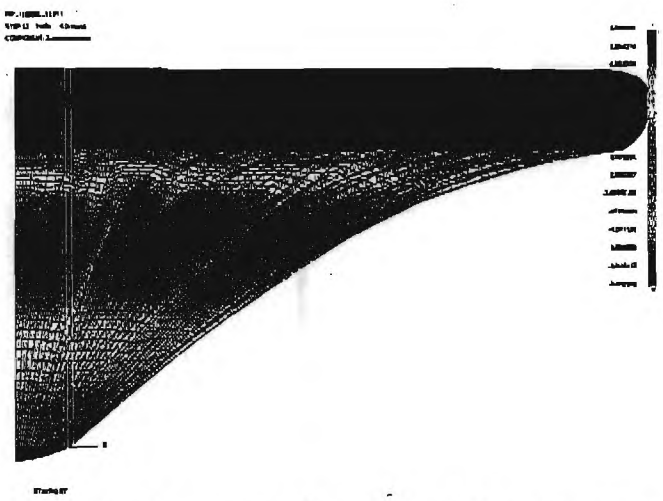

Fig. 3: Grid used for structural modeling of ISP wind tunnel test.

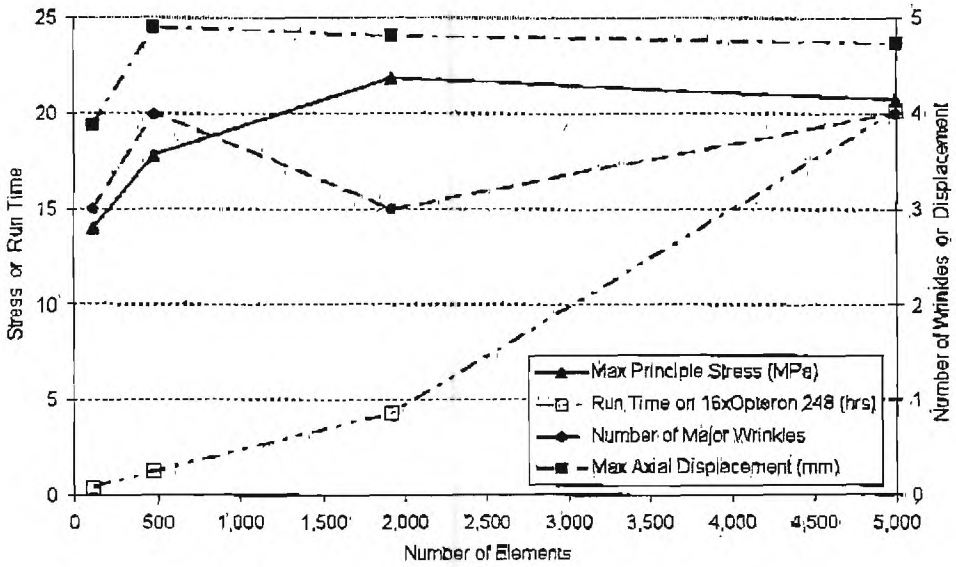

Fig. 4: Grid refinement metrics showing good convergence.

Coupled Low-Fidelity Aerodynamics Solution

The low-fidelity aerodynamic code assumes a perfect gas. The GasEQ [22] program was used to determine the equilibrium flow properties of CF_4 at the freestream temperature of 254 K. The resulting ratio of specific heats is 1.176 and the gas constant is 94.47 J/kg-K. The coupled code was allowed to run for 6.5 sec. (13 iterations) at which point the solution had reached a steady state. The resulting deformed shape is shown in Fig. 5 with surface pressure contours. The quarter model used for computation was reflected twice to produce a complete model for visualization purposes. The large surface wrinkles observed in test (Fig. 2) are present, but the minor wrinkles between each major wrinkle are not as prominent. Looking closely at Fig. 6 shows that the membrane contour matches well except near the outer radius, where the floating support ring has moved forward in the computation and backwards in the experiment. This difference

indicates that the material must have a lower modulus (higher temperature) or expand substantially due to thermal effects. Membrane deformation in the experiment was hampered by interference with the support structure of the aft ring, but this is not expected to cause the discrepancy in aft ring movement observed.

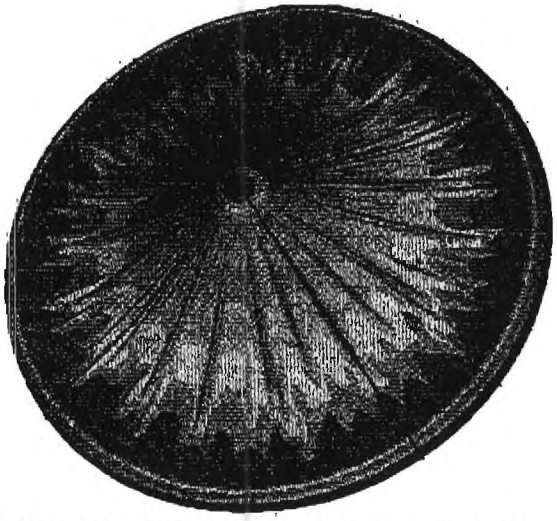

Fig. 5: Static coupled solution of the ISP wind tunnel model with surface pressure contours. Red indicates higher pressure, more blunt surfaces and dark red lines are reflection boundaries.

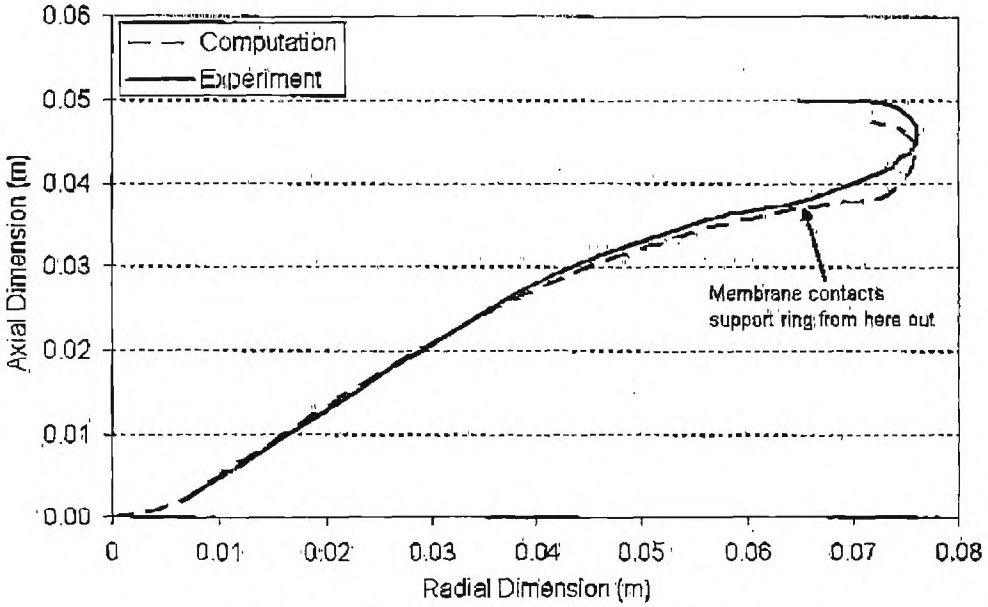

Fig. 6: Radial profile of the static coupled solution.

The discrepancy between the computed and experimental profiles is likely caused by incorrect material properties, incorrect pressure distribution, or thermal expansion. The pressure distribution produced by the low-fidelity aerodynamics does not take into account the complex shock structure observed around the body and will be addressed by using high-fidelity CFD

analysis in the following section. Incorrect material properties could be due to either material nonlinearity or an incorrect estimate of the material temperature. ILC Dover provided stress-strain data at 500°C and stress-strain data at 200°C and 23°C is from DuPont product literature [23]. The peak stress calculated for the test model is 22 MPa, which falls in the linear region of the stress-strain curve at both 23°C and 200°C. Curves were interpolated between 200°C and 500°C to estimate that the calculated peak stress of 21 MPa is still within the linear range of this material up to about 425°C. Due to the linear nature of the material in the temperatures explored, material nonlinearity does not account for the discrepancy.

Models were run at 350°C without thermal expansion and at 260°C with thermal expansion. The addition of thermal expansion causes the support ring to move aft, but not quite as far as the experiment. Even without thermal expansion, increasing the temperature to 350°C allows the support ring to move aft, but not as much as the addition of thermal expansion. From these two results it appears that some combination of thermal expansion and increased temperature will result in a nearly perfect match to experiment. Trial and error was used to determine the proper temperature required to match the experimental data. Figure 7 shows the profile with the best fit, which includes thermal expansion at a temperature of 300°C. Increasing the material temperature beyond 300°C did not produce additional deflection of the aft support ring and caused the excessive deflection of the membrane. This indicates that the remaining error is in the pressure distribution, the aft ring-membrane contact, or un-modeled effects such as creep. Unfortunately, in the experiment the aft ring made contact with the membrane near the outer radius. Changing the aft ring to membrane contact point changed the membrane deformation and aft ring motion. The error in the displacement of the aft support ring is in part due to this interference.

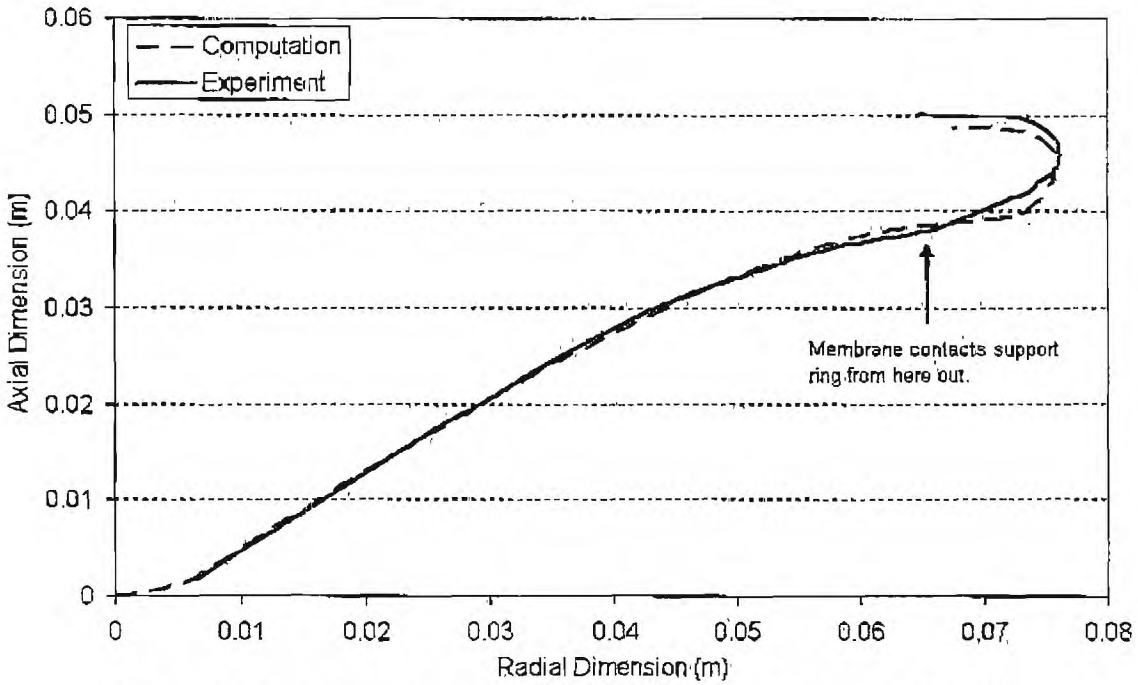

Fig. 7: The best computational solution includes thermal expansion at 300°C.

Coupled High-Fidelity Aerodynamics Solution

High-fidelity analysis was performed by coupling NASCART-GT to LS-DYNA. Preliminary grid studies were performed with NASCART-GT to determine the necessary grid resolution. Coupled analysis was then run with the best grid resolution for both NASCART-GT and LS-DYNA.

The preliminary grid studies using NASCART-GT were performed on a grid generated by sweeping the deformed profile to form a solid body. This generates an average deformed surface since it does not contain the surface wrinkle patterns. The parameter controlling the number of cells on the body in NASCART-GT (nbmin) was then varied until the proper shock structure developed. Figure 8 shows the shock structure computed by NASCART-GT with nbmin = 180 and a photograph from the wind tunnel test. The shock structure in the photograph was enhanced by applying a different color map to the image. Good agreement is observed between the computed and experimental shock structures. Further refinement was not conducted since the results agree well with experiment and the computational time would be prohibitive. Lower values of nbmin did not properly capture the shock structure around the body.

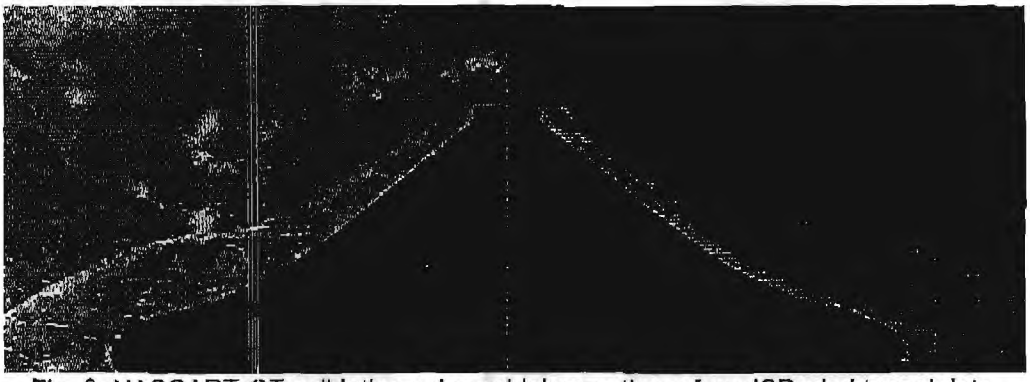

Fig. 8: NASCART-GT validation using schleiren patterns from ISP wind tunnel data.

Comparison of Low- and High-Fidelity Solutions

When NASCART-GT pressure data is used in the coupled analysis the results were essentially the same as for the modified Newtonian analysis (Fig. 9). The pressure distribution from NASCART-GT is shown in Fig. 10. The splotchy high pressure regions are a combination of interpolation from a fine computational grid to a relatively coarse structural grid and the flowfield over the relatively large surface wrinkles. Despite the substantial difference in pressure distribution due to the shock interaction over the body, the deformed profile is nearly identical. Both profiles match very well considering the orientation of the profile in the test data is unknown relative to the surface wrinkling. Three-dimensional surface contours from test data could remedy this problem, but are currently unavailable.

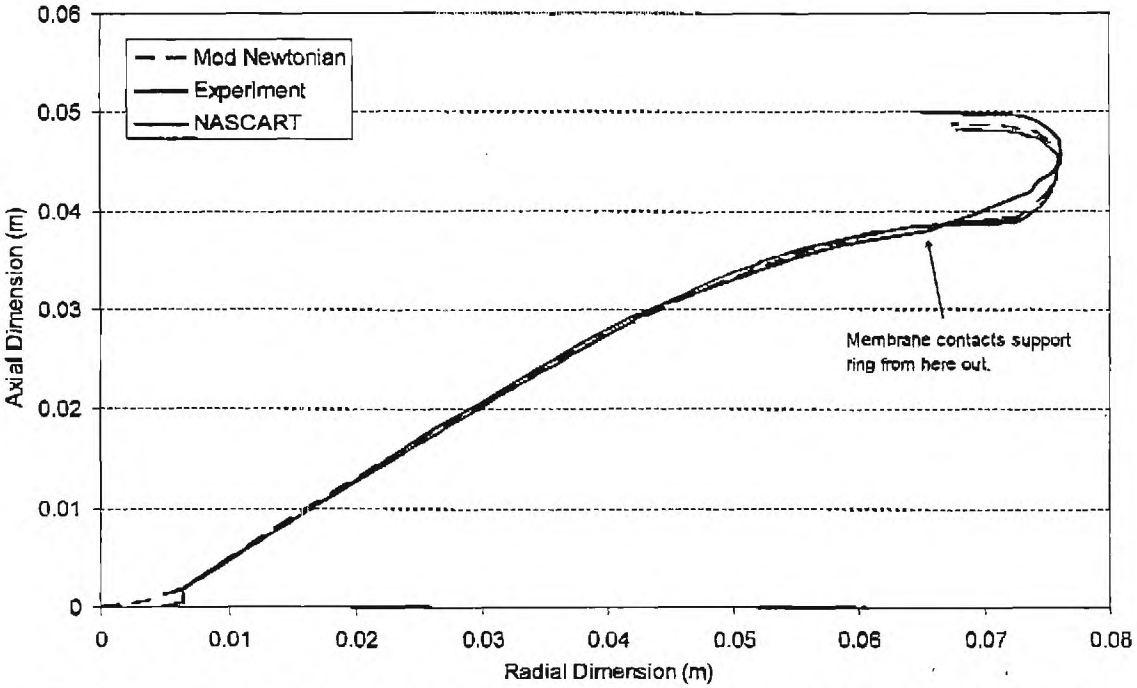

Fig. 9: Deformed profiles from NASCART-GT and modified Newtonian aerodynamics both compare well with experiment.

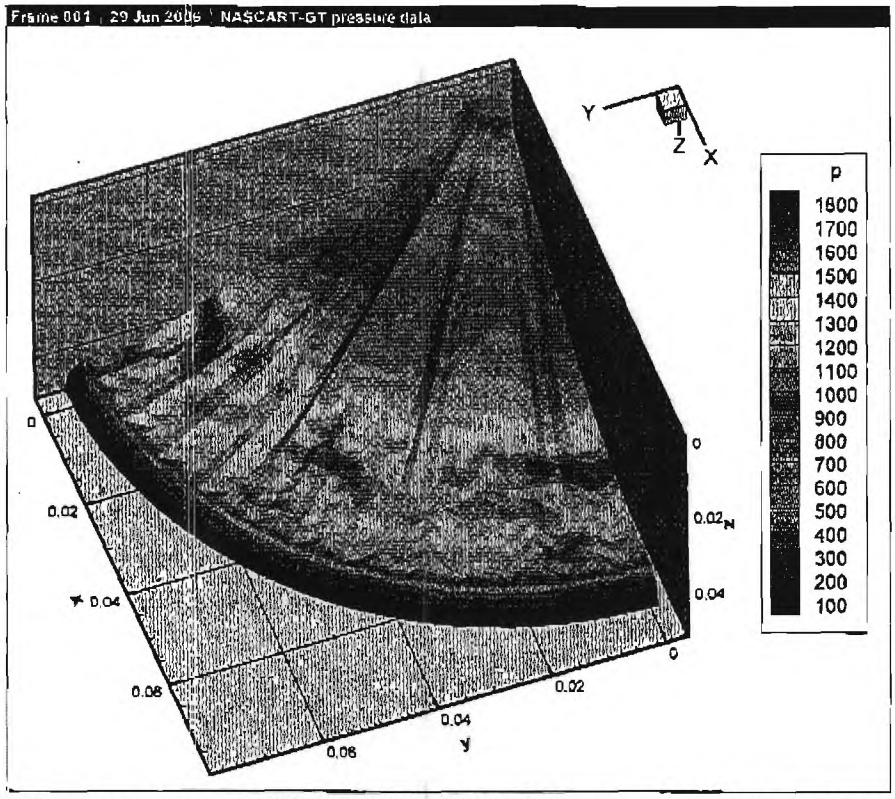

Fig. 10: Pressures computed by NASCART-GT shown on the deformed geometry.

BALLUTE STATIC AEROELASTIC ANALYSIS

Aerocapture is possible at any body with a substantial atmosphere, and is of particular interest for missions to the outer planets. Titan, in particular, has been studied extensively as a target for an aerocapture mission. The mission selected as the example problem has been documented extensively in Miller et al. [24], Johnson and Lyons [25], Westhelle and Masciarelli [26], Brown and Richardson [27], and James et al. [28].

Ballute Geometry

The configuration selected for analysis is shown in Fig. 11. Structural analysis of this configuration revealed too high a stress level near the ballute to spacecraft attach point to use a polymer membrane for the entire cone so a 3.556×10^{-4} meter thick Nextel fabric is used for the inner 6.1 meters of the cone. The remainder of the ballute is constructed of Upilex of 5.08×10^{-5} meter thickness in the cone, and 3.4×10^{-4} meter thickness in the torus. Torus thickness was determined using the buckling equations of Weeks [29] for a radial load applied horizontally at the centerline of the torus. The radial load due to aerodynamics on the conic membrane was determined using statics and the attachment angle of the cone after deformation. Fill pressure was chosen to counter the circumferential stress in the torus with a small margin, resulting in a fill pressure of 720 Pa.

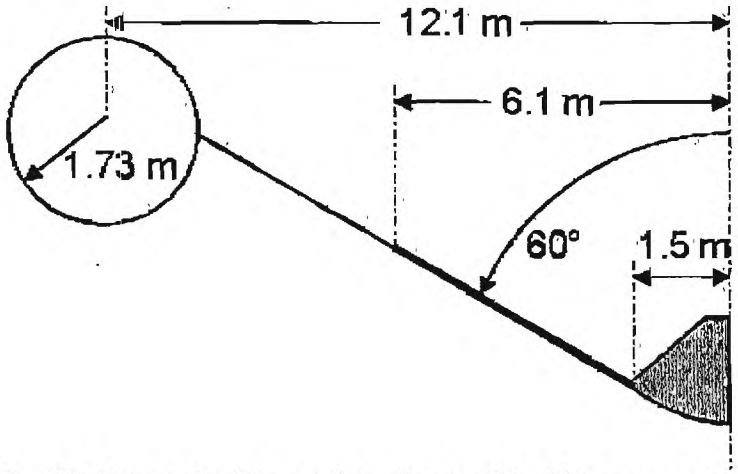

Fig. 11: Clamped ballute configuration used for Titan aerocapture.

The chosen configuration was modeled in LS-DYNA using quadrilateral shell elements. A grid convergence study was performed with this model using a fixed aerodynamic load based on the initial geometry. Convergence was based on axial displacement and principle stress. Figure 12 shows that the model with 22,464 elements was adequately refined. The selected grid is shown in Fig. 13 in the deformed configuration.

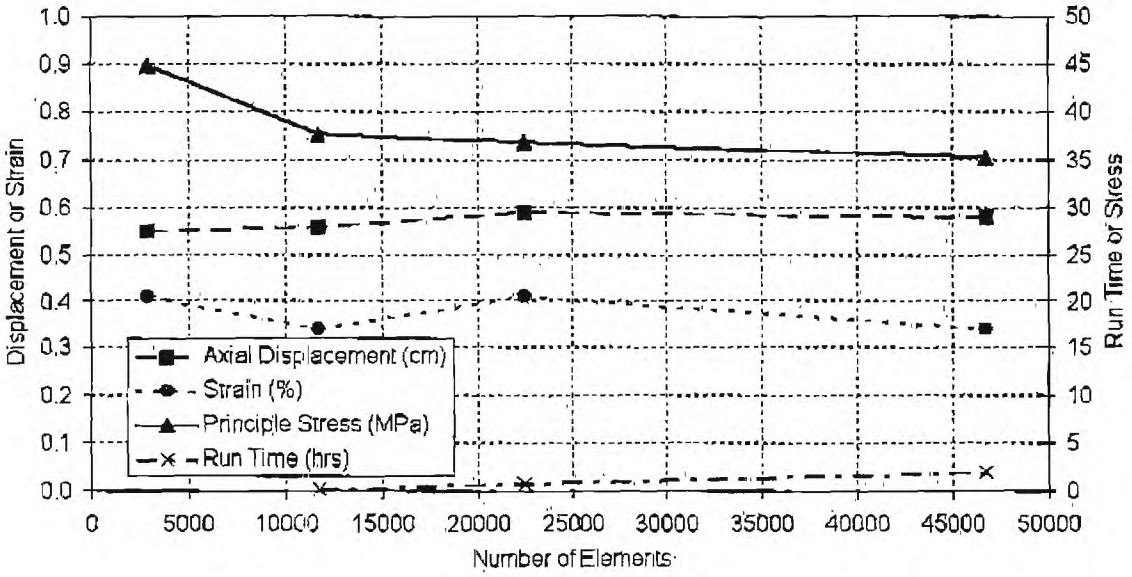

Fig. 12: Grid metrics showing grid convergence for the model with 22,464 elements.

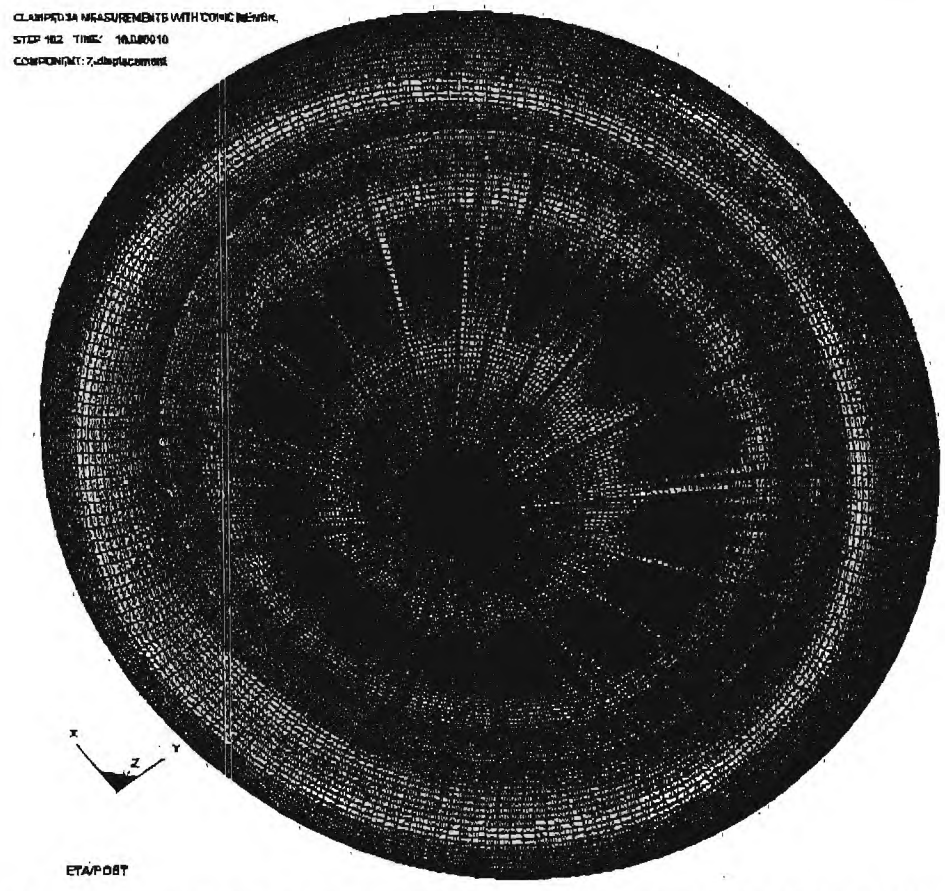

Fig. 13: The converged grid showing axial deformation. Red indicates larger displacement.

Ballute Trajectory

The trajectory used in this study was computed for a 1,000 kg spacecraft inserting into a 1,000 km circular orbit about Titan with an entry velocity of 8 km/s. The trajectory is bounded on the steep side by a heat rate limit of 3 W/cm^2 and on the shallow limit by the minimum velocity change required to insert into a 1,000 km altitude circular orbit. Aeroelastic solutions will be calculated at two points on the steep aerocapture trajectory because the steep trajectory produces the highest aerodynamic loads. The peak dynamic pressure point will be analyzed since it is the highest loading on the trajectory, and a point in the transitional regime will be analyzed. The two points chosen are shown in Table 3. All aerodynamic analysis presented in this paper assumes a perfect gas with a constant ratio of specific heats.

Table 3: Trajectory data for two points on a Titan aerocpature trajectory.

	Peak Dyn. Pressure Point	**Transitional Point**
Velocity (m/s)	4,266.4	6,512.0
Density (kg/m3)	5.66×10^{-6}	2.05×10^{-8}
Temperature (K)	166	202
Pressure (Pa)	1.22×10^{-3}	2.73×10^{-1}
γ	1.424	1.416
Gas Constant (J/kg-K)	286.9	288.6
Knudsen Number	0.00233	0.9994

Coupled Low-Fidelity Aerodynamics Solutions

The two trajectory points listed above were both run using the low-fidelity aerodynamics tools to estimate the deformation. Both points fall in the transitional regime and will use the bridging function to compute surface pressures.

Ballute temperature is only known at the peak dynamic pressure point and is applied to the ballute as a uniform temperature of 228°C. For the transitional point the temperature is unknown and so is estimated at 100°C for the purpose of this study. The temperature data is applied only to the material properties to produce a lower modulus material. Thermal expansion was not included in these models since it produced a numerical instability for which a solution has not been found. More work is necessary in the area of thermal modeling to determine both the actual ballute temperature and to include thermal expansion effects. The properties of Upilex SN are listed in Table 4 at the two temperatures used. The properties of Nextel fabric are essentially constant over the temperature range of interest with a modulus of 7 GPa, a Poisson ratio of 0.20, and a yield stress of 1.7 GPa.

Table 4: Material properties of Upilex.

	100°C	**228°C**
Modulus (GPa)	4.692	3.883
Poisson Ratio	0.34	0.34
Yield Stress (MPa)	210	130

The peak dynamic pressure case is nearly in the continuum and primarily derives the surface pressure from modified Newtonian analysis. The resulting axial displacement of the torus is

0.21 meters and the maximum VonMises stress is 35.2 MPa, well below the yield stress. Table 5 lists the tracked metrics for the peak dynamic pressure point analysis. The deformed shape with surface pressure contours is shown in Fig. 14.

Table 5: Metrics for the clamped ballute at peak dynamic pressure.

Axial deflection of torus (m)	0.21
Max VonMises Stress (MPa)	35.2
Max strain (%)	0.35
Nose pressure (Pa)	94.4
Drag (N)	10,001

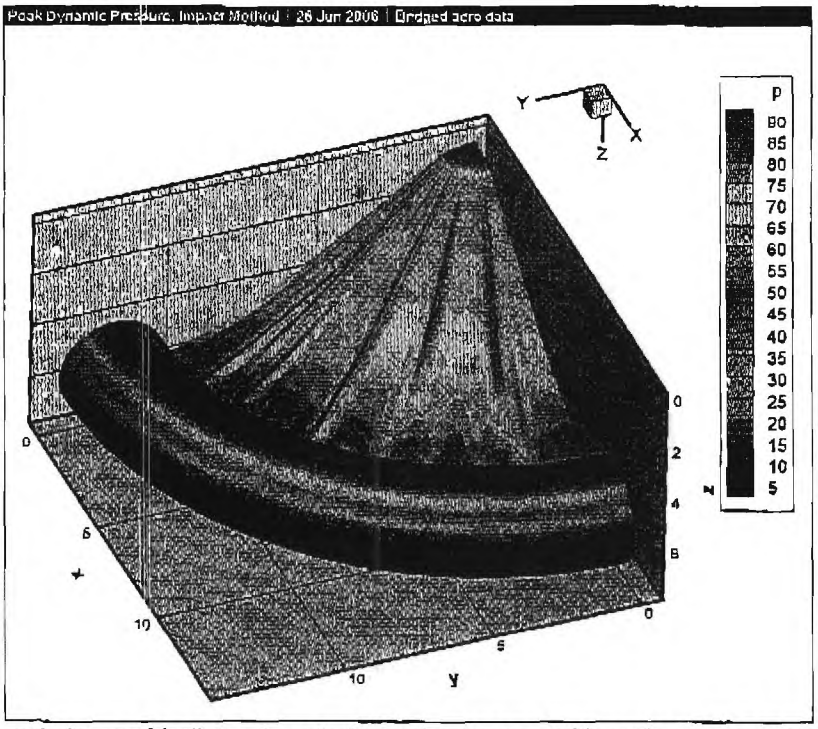

Fig. 14: Deformed clamped ballute at peak dynamic pressure with surface pressure contours in Pa.

The transitional regime case is nearly in the rarefied regime and is mostly influenced by the collisionless DSMC calculation. Due to the substantially lower atmospheric density the axial deflection of the torus is only -0.03 meters and the maximum principle stress is 4.08 MPa. The deformed shape with surface pressure contours is shown in Fig. 15. At this flight condition the pressure is not high enough to stretch the conic membrane taught, and only the beginnings of wrinkles are apparent.

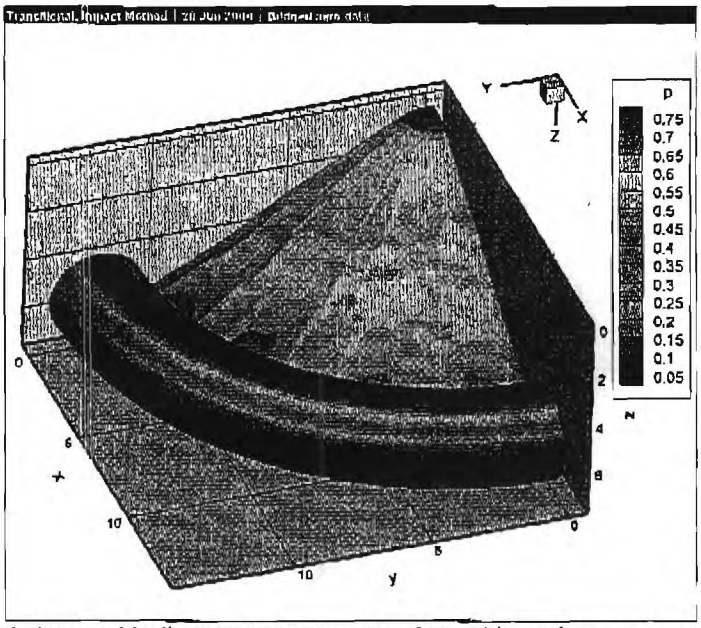

Fig. 15: Deformed clamped ballute in transitional regime with surface pressure contours in Pa.

Coupled High-Fidelity Aerodynamics Solutions

The transitional case was run using the DAC software as a point of comparison for the low-fidelity aerodynamics tool. The resulting deformation is shown in Fig. 16 with surface pressure contours on the body and temperature contours on the flowfield slice. The bow shock stands about 3.5 meters in front of the vehicle nose, which is out of the computational domain in this analysis. Previous computations were performed to determine the minimum computational domain and execution time necessary to obtain accurate surface pressures.

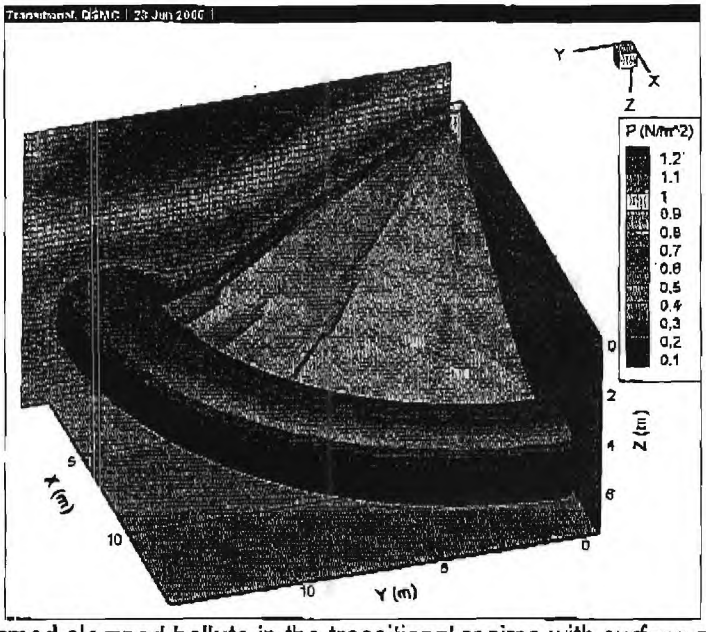

Fig. 16: The deformed clamped ballute in the transitional regime with surface pressure contours and flowfield temperature.

Comparison of Low- and High-Fidelity Solutions

At the transitional regime point on the trajectory, analysis was performed using both low-fidelity impact methods and DSMC aerodynamics. Several significant differences are observed including the torus axial deflection and the peak VonMises stress in the membrane (Table 6). These two differences are both a result of the high pressure region near the torus-cone attachment point in the DSMC calculations. This high pressure produces more bending in the conic membrane which leads to the torus moving forward and a higher stress in the conic membrane where the wrinkles bend. Despite the differences, the predicted drag is within 4% which is sufficiently accurate for preliminary trajectory analysis.

Table 6: Comparison of low- and high-fidelity coupled solutions.

	Collisionless DSMC	**DSMC**
Axial deflection of torus (m)	-0.03	-0.15
Max VonMises Stress (MPa)	4.08	3.5
Max strain (%)	0.06	0.08
Nose pressure (Pa)	0.80	0.90
Drag (N)	137	132

CONCLUSIONS

This research focused on development and application of a new tool for ballute aeroelastic analysis (BAAT) and computations of the static deformed shape of a ballute in hypersonic flight. Good agreement was obtained with validation data when using modified Newtonian aerodynamics or CFD, when including temperature dependent material properties and thermal expansion. BAAT was used to calculate the deformed shape of a ballute at two points on a Titan aerocapture trajectory, one at peak dynamic pressure and the other in the transitional regime. The resulting deformation and stress indicate that the ballute could survive the flight environment, but heating has not yet been properly computed. Comparison of the impact method aerodynamics and DSMC in the transitional regime indicate that the impact method is sufficient for trajectory analysis (reasonable drag prediction) but not for determining survivability.

REFERENCES

[1] Andrews, D.G., and Bloetscher, F., "Aerobraked Orbital Transfer Vehicle Definition," AIAA Paper 81-0279, 19th Aerospace Sciences Meeting, St. Louis, MO, Jan. 12-15 1981.

[2] Grenich, A.F., and Woods, W.C., "Flow Field Investigation of Atmospheric Braking for High Drag Vehicles with Forward Facing Jets in Spacecraft Entry," AIAA Paper 91-0293, 19th Aerospace Sciences Meeting, St. Louis, MO, Jan. 12-15 1981.

[3] McRonald, A.D., "A Light-Weight Inflatable Hypersonic Drag Device for Planetary Entry," AIAA Paper 99-0422, Association Aeronautique de France Converence, Arcachon, France, Mar. 16-18, 1999.

[4] Rohrschneider, R.R., and Braun, R.D., "Survey of Ballute Technology for Aerocapture," Accepted for publication in the *Journal of Spacecraft and Rockets*, 2006.
[5] Hall, J.L., "A Review of Ballute Technology for Planetary Aerocapture," AIAA Paper 2000-0382, 4th IAA Conference on Low Cost Planetary Missions, Laurel, MD, May 2-5 2000.
[6] Baum, J.D., Lua, H., Mestreau, E.L., Sharov, D., Lohner, R., Plessone, D., and Charman, C., "Recent Developments of a Coupled CFD/CSD Methodology," AIAA Paper 2001-2618, 15th AIAA Computational Fluid Dynamics Conference, Anaheim, CA, June 11-14 2001.
[7] Matthies, H.G., and Steindorf, J., "Partitioned Strong Coupling Algorithms for Fluid-Structure Interaction," *Computers & Structures*, vol. 81, no. 8-11, May 2003, pp.805-812.
[8] Bhardwaj, M.K., Kapania, R.K., Reichenbach, E., and Guruswamy, G.P., "Computational Fluid Dynamics/Computational Structural Dynamics Interaction Methodology for Aircraft Wings," AIAA Journal, vol. 36, no. 12, Dec. 1998.
[9] Bauchau, O.A., and Ahmad, J.U., "Advanced CFD and CSD Methods for Multidisciplinary Applications in Rotorcraft Problems," AIAA Paper 96-4151, 6th NASA and ISSMO Symposium on Multidisciplinary Analysis and Optimization, Bellevue, WA, Sep. 4-6 1996.
[10] Livermore Software Technology Corp., "LS-DYNA Keyword User's Manual," Version 970, 2003.
[11] Topping, A.D., "Ring Buckling of Inflated Drag Bodies," Journal of Aircraft, vol. 8, no. 11, Nov. 1970, pp.869-874.
[12] Marshall, D., and Ruffin, S.M., "A New Inviscid Wall Boundary Condition Treatment for Embedded Boundary Cartesian Grid Schemes," AIAA Paper 2004-0583, Jan. 2004.
[13] Tu, S., and Ruffin, S.M., "Solution Adaptive, Unstructured Cartesian-Grid Methodology for Chemically Reacting Flows", AIAA Paper 2002-3097, June 2002.
[14] LeBeau, G.J., and Lumpkin III, F.E., "Application Highlights of the DSMC Analysis Code (DAC) Software for Simulating Rarefied Flows," Computer Methods in Applied Mechanics and Engineering, vol. 191, no. 6-7, 2001, pp.595-609.
[15] Bird, G.A., Molecular Gas Dynamics and the Direct Simulation of Gas Flows, Oxford University Press, New York, NY, 1994.
[16] Anderson, J.D. Jr., Hypersonic and High Temperature Gas Dynamics, American Institute of Aeronautics and Astronautics, Reston, VA, 2000.
[17] Wilmoth, R.G., Blanchard, R.C., and Moss, J.N., "Rarefied Transitional Bridging of Blunt Body Aerodynamics," 21st International Symposium on Rarefied Gas Dynamics, Marseille, France, July 1998.
[18] Miller, K.L., et al., "ISP Cycle 1 Ballute Aerocapture Base Year Final Report," Ball Aerospace & Technologies Corp., Jan. 30, 2004.
[19] Moss, J.N., Blanchard, R.C., Wilmoth, R.G., and Braun, R.D., "Mars Pathfinder Rarefied Aerodynamics: Computations and Measurements," AIAA Paper 98-0298, 36th AIAA Aerospace Sciences Meeting and Exhibit, Reno, NV, Jan. 12-15 1998.
[20] Buck, G.M., "Testing of Flexible Ballutes in Hypersonic Wind Tunnels for Planetary Aerocpautre," AIAA Paper 2006-1319, 44th AIAA Aerospace Sciences Meeting and Exhibit, Reno, NV, Jan. 9-12 2006.
[21] DuPont Corp., "DuPont Kapton HN: Polyimide Film," Report K-15345, March, 2006.
[22] Morley, C., GasEQ, Version 0.79, http://www.gaseq.co.uk/ Jan. 2005.
[23] DuPont Corp., "Summary Properties for Kapton Polyimide Films," Report H-38492-1, March, 1997.
[24] Miller, K.L., Gulick, D., Lewis, J., Trochman, B., Stein, J., Lyons, D.T., and Wilmoth, R.G., "Trailing Ballute Aerocapture – Concept and Feasibility Assesment," AIAA Paper 2003-4655, 39th AIAA/ASME/SAE/ASEE Joint Propulsion Conference and Exhibit, Huntsville, AL, July 20-23 2003.
[25] Johnson, W.R., and Lyons, D.T., "Titan Ballute Aerocaputre Using a Perturbed TitanGRAM Model," AIAA Paper 2004-5280, AIAA Atmospheric Flight Mechanics Conference and Exhibit, Providence, RI, Aug. 16-19 2004.
[26] Westhelle, C.H., and Masciarelli, J.P., "Assessment of Aerocapture Flight at Titan Using a Drag-Only Device," AIAA Paper 2003-5389, AIAA Atmospheric Flight Mechanics Conference and Exhibit, Austin, TX, Aug. 11-14 2003.
[27] Brown, G.J., and Richardson, E.M., "Minimum-Mass Design for Titan Aerocapture," AIAA Paper 2004-1637, 18th AIAA Aerodynamic Decelerator Systems Technology Conference and Seminar, Munich, Germany, May 2005.
[28] James, B., Munk, M., and Moon, S., "Aerocapture Technology Project Overview," AIAA Paper 2003-4654, 39th AIAA/ASME/SAE/ASEE Joint Propulsion Conference and Exhibit, Huntsville, AL, July 20-23 2003.
[29] Weeks, G.E., "Buckling of a Pressurized Toroidal Ring Under Uniform External Loading," NASA-TN-D-4124, Aug. 1967.